

# Semileptonic decays $\Lambda_c^+ \rightarrow \Lambda \ell^+ \nu_\ell$ ( $\ell = e, \mu$ ) in the covariant quark model and comparison with the new absolute branching fraction measurements of Belle and BESIII

Thomas Gutsche,<sup>1</sup> Mikhail A. Ivanov,<sup>2</sup> Jürgen G. Körner,<sup>3</sup> Valery E. Lyubovitskij,<sup>1,4,5</sup> and Pietro Santorelli<sup>6,7</sup>

<sup>1</sup> *Institut für Theoretische Physik, Universität Tübingen,*

*Kepler Center for Astro and Particle Physics, Auf der Morgenstelle 14, D-72076, Tübingen, Germany*

<sup>2</sup> *Bogoliubov Laboratory of Theoretical Physics, Joint Institute for Nuclear Research, 141980 Dubna, Russia*

<sup>3</sup> *PRISMA Cluster of Excellence, Institut für Physik,*

*Johannes Gutenberg-Universität, D-55099 Mainz, Germany*

<sup>4</sup> *Department of Physics, Tomsk State University, 634050 Tomsk, Russia*

<sup>5</sup> *Mathematical Physics Department, Tomsk Polytechnic University, Lenin Avenue 30, 634050 Tomsk, Russia*

<sup>6</sup> *Dipartimento di Fisica, Università di Napoli Federico II,*

*Complesso Universitario di Monte Sant' Angelo, Via Cintia, Edificio 6, 80126 Napoli, Italy*

<sup>7</sup> *Istituto Nazionale di Fisica Nucleare, Sezione di Napoli, 80126 Napoli, Italy*

We present precise theoretical predictions for the absolute branching fractions of  $\Lambda_c^+ \rightarrow \Lambda \ell^+ \nu_\ell$  ( $\ell = e, \mu$ ) decays in the covariant confined quark model. This study is motivated by two recent and accurate measurements of the absolute branching fractions of  $\Lambda_c^+ \rightarrow p K^- \pi^+$  and  $\Lambda_c^+ \rightarrow \Lambda e^+ \nu_e$  by the Belle Collaboration at the KEKB and by the BESIII Collaboration at the BEPCII. Our predictions for the branching fractions are consistent with both experimental results. We also provide detailed numerical results for differential decay distributions and polarization observables.

PACS numbers: 12.39.Ki, 13.30.Eg, 14.20.Jn, 14.20.Lq

Keywords: relativistic quark model, light and heavy baryons, decay rates and asymmetries

## I. INTRODUCTION

In 2013 the Belle Collaboration at KEKB [1] reported on the first model-independent measurement of the branching fraction  $\text{Br}(\Lambda_c^+ \rightarrow p K^- \pi^+) = (6.84 \pm 0.24^{+0.21}_{-0.27})\%$ . This measurement significantly improved the precision of the absolute branching fractions of other  $\Lambda_c^+$  decay modes and of  $b$ -flavored hadrons involving the  $\Lambda_c^+$  state. In particular, using the Belle result the Particle Data Group [2] updated their average for the branching fractions of the exclusive semileptonic modes of the  $\Lambda_c^+$  to

$$\begin{aligned} \text{Br}(\Lambda_c^+ \rightarrow \Lambda e^+ \nu_e) &= (2.9 \pm 0.5)\%, \\ \text{Br}(\Lambda_c^+ \rightarrow \Lambda \mu^+ \nu_\mu) &= (2.7 \pm 0.6)\%. \end{aligned} \quad (1)$$

A few months ago the BESIII Collaboration reported on the first absolute measurement of the branching ratio of  $\Lambda_c^+ \rightarrow \Lambda e^+ \nu_e = (3.63 \pm 0.38(\text{stat}) \pm 0.20(\text{syst}))\%$  [3]. The current upper limit, given in the 2015 Review of Particle Physics, agrees with the lower limit of the BESIII result. The new data calls for a detailed theoretical analysis of the  $\Lambda_c^+ \rightarrow \Lambda \ell^+ \nu_\ell$  ( $\ell = e, \mu$ ) process.

In this paper we present a comprehensive study of the semileptonic decay  $\Lambda_c^+ \rightarrow \Lambda \ell^+ \nu_\ell$  in the covariant confined quark model [4]–[9]. We calculate the total rate, differential decay distributions and polarization effects. The paper is organized as follows. In Sec. II, we briefly review the helicity formalism for the  $\Lambda_c \rightarrow \Lambda$  transition which was discussed in detail e.g. in Ref. [9]. In Sec. III we discuss the dynamics of the current-induced  $\Lambda_c \rightarrow \Lambda$  transitions in terms of the covariant confined quark model and present our numerical results. Finally, in Sec. IV we

summarize and conclude our results.

## II. HELICITY FORMALISM FOR THE $\Lambda_c \rightarrow \Lambda$ TRANSITION

First we define the matrix element  $M_\mu^{V/A}(\lambda_1, \lambda_2) = \langle B_2, \lambda_2 | J_\mu^{V/A} | B_1, \lambda_1 \rangle$  of the process  $\Lambda_c^+(p_1) \rightarrow \Lambda^0(p_2) + W_{\text{off-shell}}^+(q)$ , which can be expanded in terms of a complete set of invariants

$$\begin{aligned} M_\mu^V(\lambda_1, \lambda_2) &= \bar{u}_2(p_2, \lambda_2) \left[ F_1^V(q^2) \gamma_\mu - \frac{F_2^V(q^2)}{M_1} i \sigma_{\mu q} \right. \\ &\quad \left. + \frac{F_3^V(q^2)}{M_1} q_\mu \right] u_1(p_1, \lambda_1), \end{aligned} \quad (2)$$

$$\begin{aligned} M_\mu^A(\lambda_1, \lambda_2) &= \bar{u}_2(p_2, \lambda_2) \left[ F_1^A(q^2) \gamma_\mu - \frac{F_2^A(q^2)}{M_1} i \sigma_{\mu q} \right. \\ &\quad \left. + \frac{F_3^A(q^2)}{M_1} q_\mu \right] \gamma_5 u_1(p_1, \lambda_1), \end{aligned}$$

where  $\sigma_{\mu q} = \frac{i}{2}(\gamma_\mu \not{q} - \not{q} \gamma_\mu)$  and  $q = p_1 - p_2$ . The labels  $\lambda_i = \pm \frac{1}{2}$  denote the helicities of the two baryons. In the present application  $B_1 = \Lambda_c$  and  $B_2 = \Lambda$ .

Helicity amplitudes for the  $\Lambda_c^+ \rightarrow \Lambda^0 + W_{\text{off-shell}}^+$  transition are defined through the matrix elements as

$$H_{\lambda_2, \lambda_W}^{V/A} = M_\mu^{V/A}(\lambda_1, \lambda_2) \epsilon^{\dagger \mu}(\lambda_W), \quad (3)$$

where there are four helicities for the  $W_{\text{off-shell}}^+$ , namely  $\lambda_W = \pm 1, 0$  ( $J = 1$ ) and  $\lambda_W = 0$  ( $J = 0$ ). See Fig. 1 for

the definition of the kinematical variables for the decay process (the polar angles  $\theta$ ,  $\theta_B$  and the azimuthal angle  $\chi$ ). The label  $J = 1, 0$  denotes the two angular momenta of  $W_{\text{off-shell}}^+$  in its rest frame. Following the convention of Refs. [10, 11] we distinguish the two  $\lambda_W = 0$  states and adopt the notation  $\lambda_W = 0$  for  $J = 1$  and  $\lambda_W = t$  for  $J = 0$  ( $t$  for temporal). From angular momentum conservation one has  $\lambda_1 = \lambda_2 - \lambda_W$ . Using Eq. (3) one can derive explicit relations between the helicity amplitudes and the relativistic form factors [6]-[9]

$$\begin{aligned} H_{+\frac{1}{2}t}^{V/A} &= \frac{\sqrt{Q_{\pm}}}{\sqrt{q^2}} \left( M_{\mp} F_1^{V/A} \pm \frac{q^2}{M_1} F_3^{V/A} \right), \\ H_{+\frac{1}{2}+1}^{V/A} &= \sqrt{2Q_{\mp}} \left( F_1^{V/A} \pm \frac{M_{\pm}}{M_1} F_2^{V/A} \right), \\ H_{+\frac{1}{2}0}^{V/A} &= \frac{\sqrt{Q_{\mp}}}{\sqrt{q^2}} \left( M_{\pm} F_1^{V/A} \pm \frac{q^2}{M_1} F_2^{V/A} \right), \end{aligned} \quad (4)$$

where  $M_{\pm} = M_1 \pm M_2$  and  $Q_{\pm} = M_{\pm}^2 - q^2$ .

The total left-chiral helicity amplitude is defined by the composition

$$H_{\lambda_2, \lambda_W} = H_{\lambda_2, \lambda_W}^V - H_{\lambda_2, \lambda_W}^A, \quad (5)$$

where from parity or from an explicit calculation one has

$$H_{-\lambda_2, -\lambda_W}^V = H_{\lambda_2, \lambda_W}^V, \quad H_{-\lambda_2, -\lambda_W}^A = -H_{\lambda_2, \lambda_W}^A. \quad (6)$$

The polarization observables to be discussed further on can be expressed in terms of helicity structure functions given in terms of bilinear combinations of helicity amplitudes. The definition of the structure functions are collected in Table I (for more details see Ref. [9]).

The helicity structure functions have definite parity properties as indicated in Table I. The upper and lower halves of Table I list the parity-conserving (p.c.) and parity-violating (p.v.) bilinear combinations of helicity amplitudes, respectively, i.e. the p.c. and p.v. helicity structure functions are linked to the products of  $VV$  and  $AA$ , and  $VA$  and  $AV$  currents, respectively.

The helicity amplitudes  $H_{\lambda_2, \lambda_W}$  are a superposition of vector and axial vector pieces and thus do not have definite parity properties. One can project back to the vector and axial vector helicity amplitudes by defining the transversity amplitudes [12] (see the relations in Ref. [9]).

We do not list the full three-fold angular decay distribution of the cascade decay  $\Lambda_c \rightarrow \Lambda(\rightarrow p\pi^-) + \ell^+ \nu_\ell$  but distill various asymmetries and polarization observables from the angular decay distribution as has been done in [9]. When transcribing the results of [9] to the case  $\Lambda_c \rightarrow \Lambda \ell^+ \nu_\ell$  treated here one has to take into account the necessary changes going from the  $\ell^- \bar{\nu}_\ell$  to the  $\ell^+ \nu_\ell$  final state lepton configuration as discussed in [9].

Next we list the expressions for the physical observables (width, differential rate, polarizations) in terms of the helicity structure functions:

i) The normalized differential rate reads

$$\frac{d\Gamma}{dq^2} = \Gamma_0 \frac{(q^2 - m_\ell^2)^2 |\mathbf{p}_2|}{M_1^7 q^2} \mathcal{H}_{\text{tot}} \quad (7)$$

TABLE I: Definition of helicity structure functions

parity-conserving (p.c.)
$\mathcal{H}_U =  H_{+\frac{1}{2}+1} ^2 +  H_{-\frac{1}{2}-1} ^2$
$\mathcal{H}_L =  H_{+\frac{1}{2}0} ^2 +  H_{-\frac{1}{2}0} ^2$
$\mathcal{H}_S =  H_{+\frac{1}{2}t} ^2 +  H_{-\frac{1}{2}t} ^2$
$\mathcal{H}_{LT} = \text{Re} \left( H_{+\frac{1}{2}+1} H_{-\frac{1}{2}0}^\dagger + H_{+\frac{1}{2}0} H_{-\frac{1}{2}-1}^\dagger \right)$
$\mathcal{H}_{ST} = \text{Re} \left( H_{+\frac{1}{2}+1} H_{-\frac{1}{2}t}^\dagger + H_{+\frac{1}{2}t} H_{-\frac{1}{2}-1}^\dagger \right)$
$\mathcal{H}_{SL} = \text{Re} \left( H_{+\frac{1}{2}0} H_{+\frac{1}{2}t}^\dagger + H_{-\frac{1}{2}0} H_{-\frac{1}{2}t}^\dagger \right)$
parity-violating (p.v.)
$\mathcal{H}_P =  H_{+\frac{1}{2}+1} ^2 -  H_{-\frac{1}{2}-1} ^2$
$\mathcal{H}_{SLP} = \text{Re} \left( H_{+\frac{1}{2}0} H_{+\frac{1}{2}t}^\dagger - H_{-\frac{1}{2}0} H_{-\frac{1}{2}t}^\dagger \right)$
$\mathcal{H}_{LP} =  H_{+\frac{1}{2}0} ^2 -  H_{-\frac{1}{2}0} ^2$
$\mathcal{H}_{SP} =  H_{+\frac{1}{2}t} ^2 -  H_{-\frac{1}{2}t} ^2$
$\mathcal{H}_{LTP} = \text{Re} \left( H_{+\frac{1}{2}+1} H_{-\frac{1}{2}0}^\dagger - H_{+\frac{1}{2}0} H_{-\frac{1}{2}-1}^\dagger \right)$
$\mathcal{H}_{STP} = \text{Re} \left( H_{+\frac{1}{2}+1} H_{-\frac{1}{2}t}^\dagger - H_{+\frac{1}{2}t} H_{-\frac{1}{2}-1}^\dagger \right)$

where

$$\mathcal{H}_{\text{tot}} = \mathcal{H}_U + \mathcal{H}_L + \delta_\ell \left[ \mathcal{H}_U + \mathcal{H}_L + 3\mathcal{H}_S \right] \quad (8)$$

and where we define a helicity flip factor  $\delta_\ell = m_\ell^2/(2q^2)$ . In (7) we have introduced the Born term rate

$$\Gamma_0 = \frac{G^2 |V_{cs}|^2 M_1^5}{192\pi^3}. \quad (9)$$

The rate  $\Gamma_0$  represents the SM rate of the decay of a massive parent fermion into three massless fermions, i.e.  $M_1 \neq 0$  and  $M_2, m_\ell, m_{\nu_\ell} = 0$ , where  $F_1^{V/A} = 1$  and  $F_{2,3}^{V/A} = 0$ . The  $q^2$ -dependent factor multiplying  $\Gamma_0$  in Eq. (7) is chosen such that the integral results in 1 for these mass and form factor settings.  $V_{cs} = 0.986$  is the Cabibbo-Kobayashi-Maskawa matrix element.

It is convenient to define partial rates  $d\Gamma_X/dq^2$  and  $d\tilde{\Gamma}_X/dq^2$  for the helicity nonflip (nf) and helicity flip (hf) helicity structure functions  $\mathcal{H}_X$  defined in Table I. One has

$$\begin{aligned} \frac{d\Gamma_X}{dq^2}(\text{nf}) &= \Gamma_0 \frac{(q^2 - m_\ell^2)^2 |\mathbf{p}_2|}{M_1^7 q^2} \mathcal{H}_X, \\ \frac{d\tilde{\Gamma}_X}{dq^2}(\text{hf}) &= \delta_\ell \Gamma_0 \frac{(q^2 - m_\ell^2)^2 |\mathbf{p}_2|}{M_1^7 q^2} \mathcal{H}_X. \end{aligned} \quad (10)$$

The partial rates can then be split into a helicity “nf” and helicity “hf” part according to

$$\frac{d\Gamma_X}{dq^2} = \frac{d\Gamma_X}{dq^2}(\text{nf}) + \frac{d\tilde{\Gamma}_X}{dq^2}(\text{hf}). \quad (11)$$

ii) The lepton-side forward-backward asymmetry defined by

$$A_{FB}^\ell(q^2) = \frac{3}{4} \frac{\mathcal{H}_P - 4\delta_\ell \mathcal{H}_{SL}}{\mathcal{H}_{\text{tot}}}. \quad (12)$$

iii) The convexity parameter  $C_F(q^2)$  according to

$$C_F(q^2) = \frac{3}{4} (1 - 2\delta_\ell) \frac{\mathcal{H}_U - 2\mathcal{H}_L}{\mathcal{H}_{\text{tot}}}. \quad (13)$$

iv) Longitudinal  $P_z^h(q^2)$  and transverse  $P_x^h(q^2)$  polarizations of the daughter baryon  $\Lambda$

$$P_z^h(q^2) = \frac{\mathcal{H}_P + \mathcal{H}_{LP} + \delta_\ell (\mathcal{H}_P + \mathcal{H}_{LP} + 3\mathcal{H}_{SP})}{\mathcal{H}_{\text{tot}}},$$

$$P_x^h(q^2) = \frac{3\pi}{4\sqrt{2}} \frac{\mathcal{H}_{LT} + 2\delta_\ell \mathcal{H}_{STP}}{\mathcal{H}_{\text{tot}}}. \quad (14)$$

v) Longitudinal  $P_z^\ell(q^2)$  and transverse  $P_x^\ell(q^2)$  polarizations of the charged lepton  $\ell^+$

$$P_z^\ell(q^2) = \frac{\mathcal{H}_U + \mathcal{H}_L - \delta_\ell (\mathcal{H}_U + \mathcal{H}_L + 3\mathcal{H}_S)}{\mathcal{H}_{\text{tot}}},$$

$$P_x^\ell(q^2) = -\frac{3\pi}{4\sqrt{2}} \sqrt{\delta_\ell} \frac{\mathcal{H}_P + 2\mathcal{H}_{SL}}{\mathcal{H}_{\text{tot}}} \quad (15)$$

When calculating the  $q^2$ -averages of the components of  $\vec{P}^h$  and  $\vec{P}^\ell$  one has to reinstate the common  $q^2$ -dependent factor  $(q^2 - m_\ell^2)^2 |\mathbf{p}_2|/q^2$  in the numerator and denominator of the right hand sides of Eqs. (14) and (15).

vi) The normalized azimuthal distribution is described by

$$\widetilde{W}(\chi, q^2) = \frac{1}{2\pi} (1 + \alpha_B \gamma \cos \chi) \quad (16)$$

where

$$\gamma(q^2) = \frac{3\pi^2}{16\sqrt{2}} \frac{\mathcal{H}_{LT} + 2\delta_\ell \mathcal{H}_{STP}}{\mathcal{H}_{\text{tot}}} = \frac{\pi}{4} P_x^h(q^2) \quad (17)$$

and  $\alpha_B$  is the asymmetry parameter in the decay  $\Lambda \rightarrow p\pi^-$ .

Next we define averages of the above observables: the mean forward-backward asymmetry  $\langle A_{FB} \rangle$ , the mean convexity parameter  $\langle C_F \rangle$  and the hadronic  $\langle P_{x,z}^h \rangle$  and leptonic  $\langle P_{x,z}^\ell \rangle$  polarization components, which are ob-

tained from the nonflip and flip rates:

$$\begin{aligned} \langle A_{FB}^\ell \rangle &= \frac{3}{4} \frac{\Gamma_P - 4\tilde{\Gamma}_{SL}}{\Gamma_{\text{tot}}}, \\ \langle C_F \rangle &= \frac{3}{4} \frac{\Gamma_U - 2\Gamma_L - 2\tilde{\Gamma}_U + 4\tilde{\Gamma}_L}{\Gamma_{\text{tot}}}, \\ \langle P_z^h \rangle &= \frac{\Gamma_P + \Gamma_{LP} + \tilde{\Gamma}_P + \tilde{\Gamma}_{LP} + 3\tilde{\Gamma}_{SP}}{\Gamma_{\text{tot}}}, \\ \langle P_x^h \rangle &= \frac{3\pi}{4\sqrt{2}} \frac{\Gamma_{LT} + 2\tilde{\Gamma}_{STP}}{\Gamma_{\text{tot}}}, \\ \langle P_z^\ell \rangle &= \frac{\Gamma_U + \Gamma_L - \tilde{\Gamma}_U - \tilde{\Gamma}_L - 3\tilde{\Gamma}_S}{\Gamma_{\text{tot}}}, \\ \langle P_x^\ell \rangle &= -\frac{3\pi}{4\sqrt{2}} \sqrt{\delta_\ell} \frac{\Gamma_P + 2\Gamma_{SL}}{\Gamma_{\text{tot}}}, \\ \langle \gamma \rangle &= \frac{\pi}{4} \langle P_z^h \rangle. \end{aligned} \quad (18)$$

### III. THE $\Lambda_c \rightarrow \Lambda_s$ TRANSITION FORM FACTORS IN THE COVARIANT CONFINED QUARK MODEL

We shall use the covariant confined quark model previously developed by us to describe the dynamics of the current-induced  $\Lambda_c = (c[ud])$  to  $\Lambda_s = (s[ud])$  transition (see Refs. [5]-[9]). The starting point of the model is an interaction Lagrangian which describes the coupling of the  $\Lambda_q$ -baryon ( $q = c, s$ ) to the relevant interpolating three-quark current. One has

$$\mathcal{L}_{\text{int}}^{\Lambda_q}(x) = g_{\Lambda_q} \bar{\Lambda}_q(x) \cdot J_{\Lambda_q}(x) + \text{H.c.}, \quad (19)$$

$$J_{\Lambda_q}(x) = \int dx_1 \int dx_2 \int dx_3 F_{\Lambda_q}(x; x_1, x_2, x_3) \times \epsilon^{a_1 a_2 a_3} q^{a_1}(x_1) u^{a_2}(x_2) C \gamma^5 d^{a_3}(x_3).$$

The vertex function  $F_{\Lambda_q}$  is chosen to be of the form

$$F_{\Lambda_q} = \delta^{(4)}(x - \sum_{i=1}^3 w_i x_i) \Phi_{\Lambda_q} \left( \sum_{i < j} (x_i - x_j)^2 \right) \quad (20)$$

where  $\Phi_{\Lambda_q}$  is a correlation function involving the three constituent quarks with coordinates  $x_1, x_2, x_3$  and with masses  $m_1, m_2, m_3$ . The variable  $w_i$  is defined by  $w_i = m_i/(m_1 + m_2 + m_3)$  such that  $\sum_{i=1}^3 w_i = 1$ . The form factors describing the  $\Lambda_c \rightarrow \Lambda_s$  transition via the local weak quark current are calculated in terms of a two-loop Feynman diagram. Due to the confinement mechanism of the model, the Feynman diagrams do not contain branch points corresponding to on-shell quark production.

The values of the constituent quark masses  $m_q$  and the infrared cut-off parameter  $\lambda$  have been fixed from the analysis of a wide spectrum of data on meson and baryon decays with

$m_{u,d}$	$m_s$	$m_c$	$\lambda$	
0.241	0.428	1.67	0.181	GeV

(21)

The values of the hadronic size parameters are taken from our previous papers [6, 7]:

$$\frac{\Lambda_{\Lambda_s}}{0.492} \quad \frac{\Lambda_{\Lambda_c}}{0.867} \quad \text{GeV} \quad (22)$$

The results of our numerical two-loop calculation are well represented by a double-pole parametrization

$$F(q^2) = \frac{F(0)}{1 - as + bs^2}, \quad s = \frac{q^2}{M_1^2}. \quad (23)$$

For the  $\Lambda_c \rightarrow \Lambda_s$  transition the parameters of the approximated form of the form factors are given by

	$F_1^V$	$F_2^V$	$F_3^V$	$F_1^A$	$F_2^A$	$F_3^A$
$F(0)$	0.511	0.289	-0.014	0.466	-0.025	-0.400
$a$	1.736	1.970	5.053	1.594	0.321	2.083
$b$	0.760	1.054	8.138	0.647	8.127	1.195

(24)

Let us take a closer look at the  $q^2$  dependence of the form factors  $F_1^V(q^2) \approx F_1^A(q^2)$ . Their  $q^2$  dependence is very close to a dipole behavior since one has  $\sqrt{b} \sim a/2$  in both cases with a dipole mass  $m_{\text{dipole}} = M_1/\sqrt{a/2} \simeq 2.45$  GeV. The dipole mass is quite close to the expected  $(c\bar{s})$  mass scale of 2.1121 GeV set by the  $D_s^*$  meson mass [2].

#### IV. NUMERICAL RESULTS

We shall present numerical results for the two cases  $\ell^+ = e^+$  and  $\ell^+ = \mu^+$ . Note that the results for two modes are sometimes similar and sometimes not. In the calculations we use the baryon mass values  $M_{\Lambda_c} = 2.28646$  GeV and  $M_{\Lambda_s} = 1.11568$  GeV [2].

In Figs. 2 and 3 we display the  $q^2$ -dependence of the partial differential rates  $d\Gamma_U/dq^2$ ,  $d\Gamma_L/dq^2$  and the total differential rate  $d\Gamma_{U+L}/dq^2$  for the  $e$ - and  $\mu$ -mode. The transverse rate dominates in the low recoil region while the longitudinal rate dominates in the large recoil region. In case of the  $e$ -mode the longitudinal and thereby the total rate shows a step-like behavior close to the threshold  $q^2 = m_e^2$ .

In Fig. 4 we show the  $q^2$ -dependence of the lepton-side forward-backward asymmetry  $A_{FB}^\ell(q^2)$ , which is negative and very similar for both  $e$ - and  $\mu$ -mode at  $q^2 \geq 1$  GeV<sup>2</sup>. At zero recoil  $A_{FB}^\ell(q^2)$  goes to zero due to the zero recoil relations  $\mathcal{H}_P = \mathcal{H}_{SL} = 0$ . In the large recoil limit  $A_{FB}^e(e)$  goes to zero due to the longitudinal dominance in the partial rates.

In Fig. 5 we display the  $q^2$ -dependence of the convexity parameter  $C_F$ , which is similar for both modes for  $q^2 \geq 0.6$  GeV<sup>2</sup> and different for  $q^2 < 0.6$  GeV<sup>2</sup>. At zero

recoil  $C_F$  goes to zero for both modes due to the zero recoil relation  $\mathcal{H}_U = 2\mathcal{H}_L$ . For the  $e$ -mode one finds  $C_F \rightarrow -1.5$  at maximal recoil due to the longitudinal dominance while  $C_F \rightarrow 0$  for the  $\mu$ -mode at maximal recoil  $q^2 = m_\mu^2$  due to the overall factor  $(1 - 2\delta)$  in (13). In both modes  $C_F$  is large and negative which implies that the  $\cos\theta$ -distribution is strongly parabolic in terms of a downward open tilted parabola.

In Figs. 6 and 7 we show the longitudinal and transverse polarization components of the  $\Lambda$  defined in Eq. (14), which are similar for  $e$ - and  $\mu$ -modes in case of both polarizations. The magnitude of the  $\Lambda$  polarization shown in Fig. 8 is also similar for both modes and is quite large.

In Figs. 9 and 10 we show the  $q^2$ -dependence of the longitudinal and transverse polarization components of the charged lepton. In the case of the electron the two curves reflect the chiral limit of a massless lepton in which the lepton is purely left-handed. The behavior of the two polarization components in the  $\mu$ -mode is distinctly different. The longitudinal polarization is reduced from 1 to a negative number of  $-0.34$  at zero recoil, while the transverse polarization can become negative and quite large on magnitude towards maximal recoil. At zero recoil the transverse polarization of the charged lepton tends to zero in agreement with the vanishing of  $\mathcal{H}_P$  and  $\mathcal{H}_{SL}$  at zero recoil. The total polarization of the lepton shown in Fig. 11 is maximal in the  $e$ -mode and somewhat reduced but still quite large in the  $\mu$ -mode.

In Table II we present our predictions for the semileptonic branching ratios of the  $\Lambda_c$  in % and compare them with data from the Belle [1] and BESIII [3] Collaborations. We have used the value for the  $\Lambda_c$ -lifetime from the Particle Data Group [2]  $\tau_{\Lambda_c} = (2.0 \pm 0.06) \times 10^{-13}$  s. One can see that our results are in a good agreement with Belle data and close to the lower value of the BESIII result. In Table III we compare our predictions with previous theoretical results [4],[14]-[23] for  $\Lambda_c^+ \rightarrow \Lambda^0 e^+ \nu_e$ . For some approaches in brackets we indicate the result by taking into account the  $SU(6)$  spin-flavor suppression factor equal to 1/3 (see detailed discussion in Ref. [13]).  $q^2$ -averages of helicity structure functions in units of  $10^{-15}$  GeV are listed in Table IV. We do not display helicity flip results for the  $e^+ \nu_e$  mode because they are of order  $10^{-6} - 10^{-7}$  in the above units. Partial rates, from which we can compile the total rate, are listed in Table V. Again we list the partial and total rates in units of  $10^{-15}$  GeV. The numbers show that the partial flip rates make up 34.2 % of the total rate where the biggest contribution comes from the scalar rate with 20.4 %. The results for the mean values of the asymmetry parameters are shown in Table VI. When calculating the  $q^2$ -averages one has to remember to include the  $q^2$ -dependent factor  $(q^2 - m_\ell^2)^2 |\mathbf{p}_2|/q^2$  in the numerator and denominator of the relevant asymmetry expressions. In most of the shown cases the mean values change considerably when going from the  $e$ - to the  $\mu$ -modes including even a sign change in  $\langle A_{FB}^\ell \rangle$ .

TABLE II: Semileptonic branching ratios of the  $\Lambda_c$  in %.

Mode	Our results	Data
$\Lambda_c^+ \rightarrow \Lambda^0 e^+ \nu_e$	2.78	$(2.9 \pm 0.5)$ Belle $(3.63 \pm 0.38 \pm 0.20)$ BESIII
$\Lambda_c^+ \rightarrow \Lambda^0 \mu^+ \nu_\mu$	2.69	$(2.7 \pm 0.6)$ Belle

TABLE III: Comparison of our predictions with previous theoretical results for  $\text{Br}(\Lambda_c^+ \rightarrow \Lambda^0 e^+ \nu_e)$  in %.

Our	Ref. [14]	Ref. [15]	Ref. [16]	Ref. [17]	Ref. [18]	Ref. [19]	Ref. [20]	Ref. [4]	Ref. [21]	Ref. [22]	Ref. [23]
2.78	12 (4)	3 (1)	3.4 (1.12)	2	4.4 (1.46)	1.42	1.07	1.44	1.4	$2.64 \pm 0.36$	$3.05 \pm 0.27$
			2.6 (0.86)								$1.96 \pm 0.32$

TABLE IV:  $q^2$ -averages of helicity structure functions in units of  $10^{-15}$  GeV.

	$\Gamma_U$	$\Gamma_L$	$\Gamma_{LT}$	$\Gamma_{SL}$	$\Gamma_P$	$\Gamma_{LP}$	$\Gamma_{LTP}$				
$e^+\nu_e$	35.6	55.8	-17.7	53.9	-25.7	-53.6	-8.8				
$\mu^+\nu_\mu$	34.3	50.3	-17.1	48.5	-24.7	-48.1	-8.3				
	$\widetilde{\Gamma}_U$	$\widetilde{\Gamma}_L$	$\widetilde{\Gamma}_S$	$\widetilde{\Gamma}_{LT}$	$\widetilde{\Gamma}_{SP}$	$\widetilde{\Gamma}_{SL}$	$\widetilde{\Gamma}_P$	$\widetilde{\Gamma}_{LP}$	$\widetilde{\Gamma}_{LTP}$	$\widetilde{\Gamma}_{STP}$	$\widetilde{\Gamma}_{SLP}$
$\mu^+\nu_\mu$	0.31	0.91	0.93	-0.15	-0.90	0.91	-0.24	-0.90	-0.10	-0.19	-0.92

TABLE V: Partial rates contributing to the total rates  $\Gamma(\Lambda_c^+ \rightarrow \Lambda^0 + \ell^+ \nu_\ell)$  in units of  $10^{-15}$  GeV.

	$\Gamma_U$	$\Gamma_L$	$\tilde{\Gamma}_U$	$\tilde{\Gamma}_L$	$\tilde{\Gamma}_S$	$\Gamma_{\text{tot}}$
$e^+ \nu_e$	35.6	55.8	-	-	-	91.4
$\mu^+ \nu_\mu$	34.3	50.3	0.3	0.9	2.8	88.6

TABLE VI: Mean values of the asymmetry parameters.

	$\langle A_{FB}^\ell \rangle$	$\langle C_F \rangle$	$\langle P_z^h \rangle$	$\langle P_x^h \rangle$	$\langle P_z^\ell \rangle$	$\langle P_x^\ell \rangle$	$\langle \gamma \rangle$
$e^+ \nu_e$	-0.21	-0.62	-0.87	-0.32	1.00	-0.001	-0.25
$\mu^+ \nu_\mu$	-0.24	-0.54	-0.87	-0.33	0.91	-0.18	-0.26

## V. SUMMARY AND CONCLUSIONS

Let us summarize the main results of our paper. We have used the helicity formalism to study the angular decay distribution in the semileptonic decay  $\Lambda_c^+ \rightarrow \Lambda^0 + \ell^+ \nu_\ell$  as well as the corresponding cascade decay  $\Lambda_c^+ \rightarrow \Lambda^0 (\rightarrow p + \pi^-) + \ell^+ \nu_\ell$ . Starting from the angular decay distribution we have defined a number of polarization observables for which we have provided numerical results using form factor results from the covariant confined quark model. Our predictions for the absolute branching fractions for  $\Lambda_c^+ \rightarrow \Lambda \ell^+ \nu_\ell$  decays are in agreement with

the central value of data from Belle [1] and with the lower limit of the data from the BESIII Collaboration [3].

## Acknowledgments

This work was supported by Tomsk State University Competitiveness Improvement Program and the Russian Federation program “Nauka” (Contract No. 0.1526.2015, 3854). M.A.I. acknowledges the support from Mainz Institute for Theoretical Physics (MITP). M.A.I. and J.G.K. thank the Heisenberg-Landau Grant for support.



- [1] A. Zupanc *et al.* (Belle Collaboration), Phys. Rev. Lett. **113**, no. 4, 042002 (2014) [arXiv:1312.7826 [hep-ex]].
- [2] K. A. Olive *et al.* (Particle Data Group Collaboration), Chin. Phys. C **38**, 090001 (2014).
- [3] M. Ablikim *et al.* (BESIII Collaboration), Phys. Rev. Lett. **115**, no. 22, 221805 (2015) [arXiv:1510.02610 [hep-ex]].
- [4] M. A. Ivanov, V. E. Lyubovitskij, J. G. Körner and P. Kroll, Phys. Rev. D **56**, 348 (1997) [hep-ph/9612463].
- [5] T. Gutsche, M. A. Ivanov, J. G. Körner, V. E. Lyubovitskij and P. Santorelli, Phys. Rev. D **86**, 074013 (2012) [arXiv:1207.7052 [hep-ph]].
- [6] T. Gutsche, M. A. Ivanov, J. G. Körner, V. E. Lyubovitskij and P. Santorelli, Phys. Rev. D **87**, 074031 (2013) [arXiv:1301.3737 [hep-ph]].
- [7] T. Gutsche, M. A. Ivanov, J. G. Körner, V. E. Lyubovitskij and P. Santorelli, Phys. Rev. D **88**, 114018 (2013) [arXiv:1309.7879 [hep-ph]].
- [8] T. Gutsche, M. A. Ivanov, J. G. Körner, V. E. Lyubovitskij and P. Santorelli, Phys. Rev. D **90**, no. 11, 114033 (2014) [arXiv:1410.6043 [hep-ph]].
- [9] T. Gutsche, M. A. Ivanov, J. G. Körner, V. E. Lyubovitskij, P. Santorelli and N. Habyt, Phys. Rev. D **91**, no. 7, 074001 (2015) [Phys. Rev. D **91**, no. 11, 119907 (2015)] [arXiv:1502.04864 [hep-ph]]; N. Habyt, T. Gutsche, M. A. Ivanov, J. G. Körner, V. E. Lyubovitskij and P. Santorelli, Int. J. Mod. Phys. Conf. Ser. **39**, 1560112 (2015) [arXiv:1509.07688 [hep-ph]].
- [10] J. G. Körner and G. A. Schuler, Phys. Lett. B **231**, 306 (1989).
- [11] J. G. Körner and G. A. Schuler, Z. Phys. C **46**, 93 (1990).
- [12] F. Krüger and J. Matias, Phys. Rev. D **71**, 094009 (2005).
- [13] J. G. Körner, M. Kramer and D. Pirjol, Prog. Part. Nucl. Phys. **33**, 787 (1994) [hep-ph/9406359].
- [14] A. J. Buras, Nucl. Phys. B **109**, 373 (1976).
- [15] M. B. Gavela, Phys. Lett. B **83**, 367 (1979).
- [16] R. Perez-Marcial, R. Huerta, A. Garcia and M. Avila-Aoki, Phys. Rev. D **40**, 2955 (1989) [Phys. Rev. D **44**, 2203 (1991)].
- [17] R. L. Singleton, Phys. Rev. D **43**, 2939 (1991).
- [18] F. Hussain and J. G. Körner, Z. Phys. C **51**, 607 (1991).
- [19] H. Y. Cheng and B. Tseng, Phys. Rev. D **53**, 1457 (1996) [Phys. Rev. D **55**, 1697 (1997)].
- [20] A. Datta, hep-ph/9504429.
- [21] C. W. Luo, Eur. Phys. J. C **1**, 235 (1998).
- [22] R. S. Marques de Carvalho, F. S. Navarra, M. Nielsen, E. Ferreira and H. G. Dosch, Phys. Rev. D **60**, 034009 (1999) [hep-ph/9903326].
- [23] Y. L. Liu, M. Q. Huang and D. W. Wang, Phys. Rev. D **80**, 074011 (2009) [arXiv:0910.1160 [hep-ph]].

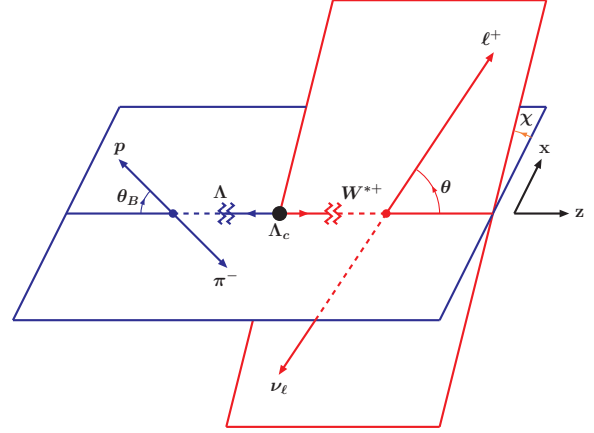


FIG. 1: Definition of the polar and the azimuthal angles.

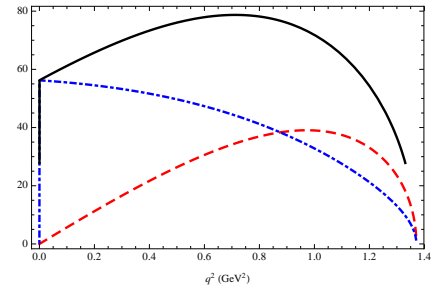


FIG. 2: The  $q^2$ -dependence of the partial rates  $d\Gamma_U/dq^2$  (dashed),  $d\Gamma_L/dq^2$  (dot-dashed) and their sum  $d\Gamma_{U+L}/dq^2$  (solid) for the  $e^+$ -mode (in units of  $10^{-15} \text{ GeV}^{-1}$ ).

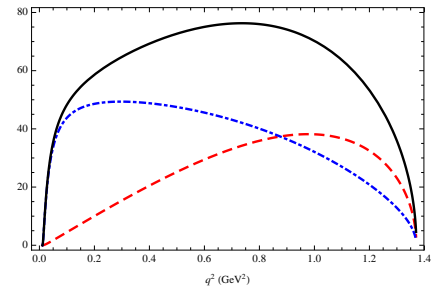


FIG. 3: The  $q^2$ -dependence of the partial rates  $d\Gamma_U/dq^2$  (dashed),  $d\Gamma_L/dq^2$  (dot-dashed) and their sum  $d\Gamma_{U+L}/dq^2$  (solid) for the  $\mu^+$ -mode (in units of  $10^{-15} \text{ GeV}^{-1}$ ).

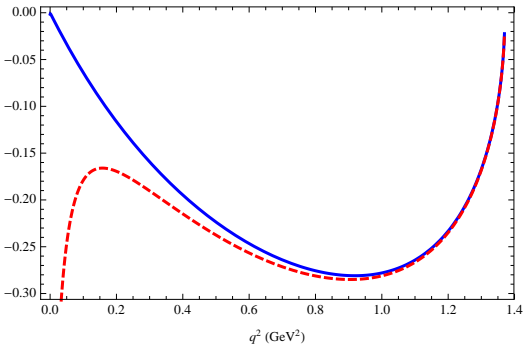


FIG. 4  $A_{FB}^\ell(q^2)$  plot:  $e^+$  (solid) and  $\mu^+$  (dashed)

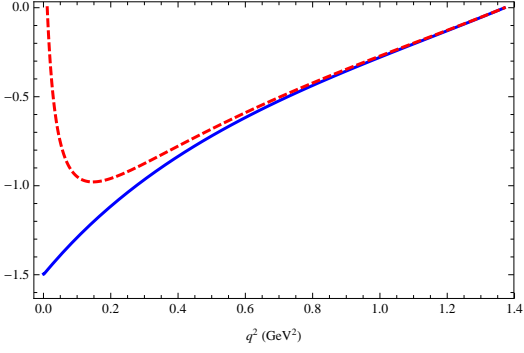


FIG. 5  $C_F(q^2)$  plot:  $e^+$  (solid) and  $\mu^+$  (dashed)

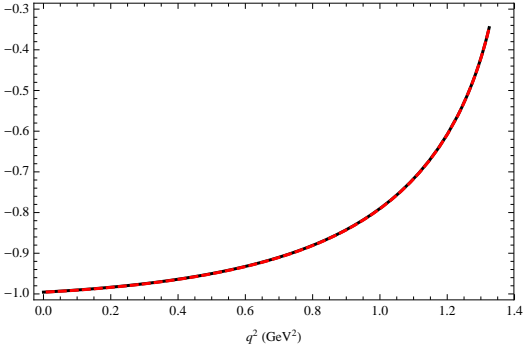


FIG. 6  $P_z^h(q^2)$  plot:  $e^+$  (solid) and  $\mu^+$  (dashed)

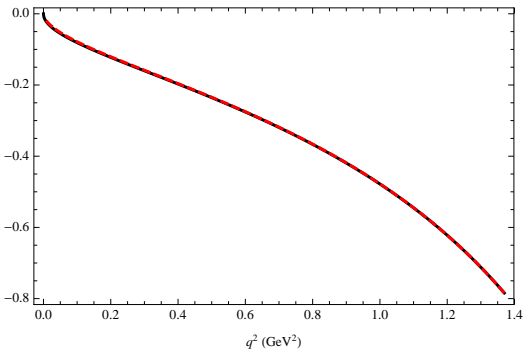


FIG. 7  $P_x^h(q^2)$  plot:  $e^+$  (solid) and  $\mu^+$  (dashed)

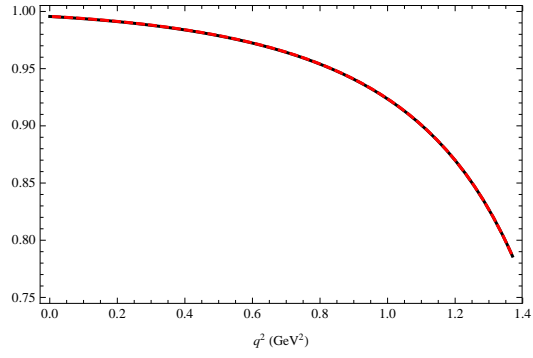


FIG. 8  $|\vec{P}^h|(q^2)$  plot:  $e^+$  (solid) and  $\mu^+$  (dashed).

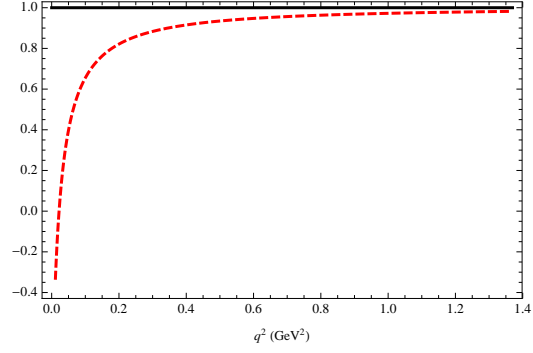


FIG. 9  $P_z^\ell(q^2)$  plot:  $e^+$  (solid) and  $\mu^+$  (dashed).

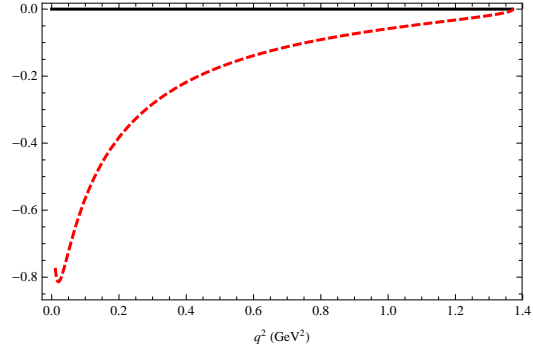


FIG. 10  $P_x^\ell(q^2)$  plot:  $e^+$  (solid) and  $\mu^+$  (dashed).

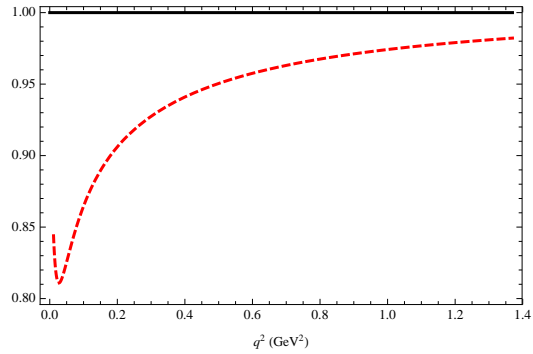


FIG. 11  $|\vec{P}^\ell|(q^2)$  plot:  $e^+$  (solid) and  $\mu^+$  (dashed).